ASIAN JOURNAL OF MATHEMATICS AND APPLICATIONS
Volume 2015, Article ID ama0264, 23 pages
ISSN 2307-7743
http://scienceasia.asia

MHD MIXED CONVECTION OF A VISCOUS DISSIPATING AND CHEMICALLY REACTING STAGNATION –POINT FLOW NEAR A VERTICAL PERMEABLE PLATE IN A POROUS MEDIUM WITH THERMAL RADIATION AND HEAT SOURCE/SINK

ADETUNJI ADENIYAN

Abstract: The particular aim of this paper is to investigate the steady laminar flow and heat transfer of a viscous incompressible electrically conducting and chemically reacting fluid permeated by a uniform transverse magnetic field over a vertical permeable linearly stretching sheet bathed in a saturated porous medium with prescribed nonlinear surface temperature, taking into account the effects of the heat source or sink, thermal radiation and Ohmic dissipation. Use was made of appropriate similarity transformations to covert the governing coupled nonlinear partial differential equations into a system of coupled nonlinear ordinary differential equations. The numerical solutions were obtained by means of the fourth order Runge-Kutta technique alongside the Newton-Raphson iteration scheme, and the results lineated on graphs and tables for selected values of various pertinent flow heat and mass transfer parameters characterizing the flow as to discuss their influences on the fluid behavior. The numerically computed results indicate that all the emerging flow parameters demonstrate very pronounced effects on the flow, mass and heat transfer characteristics.

1. Introduction

The study of flow and heat transfer consequential upon stretching sheet has a great many applications in engineering and industrial processes, essentially in polymer extrusion, fibres and films drawing, paper production, linoleum, roofing shingles, metal casting etc. Hiemenz (1911) , among his early contemporaries appeared to be the first to study two-dimensional induced flow in a boundary layer and obtained analytically, the solution of the governing Navier-Stokes equations. Much later, Sakiadis (1961) investigated the boundary layer flow due to a sheet extruding from a slit into an otherwise still fluid with a uniform velocity. Later on, many a researcher has considered various aspects of such flow with linearly stretching sheet in a quiescent or non-quiescent fluid along with different thermal boundary conditions. A few among these pioneering studies (Crane, 1970; Chamkha, 1998; Makinde et al., 2012) obtained not only closed form solutions but also the numerical ones using the similarity analysis. In several problems of heat and mass transfer convective flows concerning chemical reaction of species concentration as exemplified in petro-

2010 Mathematics Subject Classification: 80A20.
Key words and phrases: Heat generation/absorption, Magnetohydrodynamics, Ohmic dissipation, thermal radiation, stretching sheet, chemical reaction, Similarity transformation.

chemical engineering and industrial processes for drying, cleaning operations, chemical particulate deposition on surfaces, cooling towers of thermal energy plant, nuclear waste repositories, packed bed catalytic reactors, fluidized reactors, thermonuclear energy confinement, astrophysics and space science, etc. Keeping this in view, many researchers in the recent past have shown renewed interest for intensive investigations of effect of chemical reaction mechanism on boundary layer-flow for momentum, energy and mass transfer transport models. Ibrahim and Makinde (2010, 2011) investigated the effects of chemical reaction on MHD boundary layer flow over a vertically moving sheet with heat and mass transfer characteristics. The former is essentially different from the latter by the inclusion of mass wall flux velocity while Joule heating as well as chemical reaction features in the latter. Olanrewaju and Makinde (2011) conducted an analysis on free convective heat and mass transfer of an incompressible, electrically conducting and chemically reacting fluid past a stretching, porous vertical plate with Soret and Dufour effects. Ibrahim and Reddy (2013), latterly explored the simultaneous influence of internal heat generation, thermal radiation and viscous dissipation on a boundary layer flow of a chemically reacting fluid over a convectively heated vertical and uniformly moving plate. In many chemical engineering and industrial processes, chemical reactions feature between a working fluid and a foreign mass which is often associated with stress (pressure) work. However, sparse work has been done which considered this physical influence on the behavior of Newtonian boundary layer flow. Khan et al. (2003) studied viscoelastic MHD boundary layer flow, heat and mass transfer past a stretching permeable sheet with dissipation energy and stress work. Very recently, Hossain and Samand (2013) who presented the effect of radiation on thermally optically dense gray gases coupled with internal heat generation inadvertently neglected the influence of Joules heating in their similarity analysis for the scenario model of hydromagnetic boundary layer flow over a vertical permeable sheet moving nonlinearly in an electrically conducting fluid permeated by a uniform transverse magnetic field. Of late, Olanrewaju et al. (2013) analyzed through the similarity analysis the simultaneous effects of thermal and concentrations on a mixed convection boundary layer flow over a permeable surface under convective surface boundary condition in the presence of heat generation and thermal radiation. Damseh et al. (2006) reported in their study the effects of forced convection and radiative heat transfer of MHD boundary layer flow past a uniformly heated, static porous plate placed in an expanse of an electrically conducting fluid streaming uniformly in the presence of viscous dissipation and Joule heating. Makinde (2011) extended the work of Aziz (2009) by simultaneous inclusion of the influences of the magnetic field, viscous dissipation, radiative heat transfer and entropy

generation analysis. Das (2011) conducted a study of heat and mass transfer incorporating radiation and chemical reaction effects on natural convection flow of an optically thin fluid near a vertical plate. This study is devoid of viscous and Ohmic dissipations, thermal radiation and internal heat generation or absorption. Jat and Chaudhary (2009), who analyzed the stagnation-point flow with radiation over an impermeable stretching sheet in non-porous medium without consideration for heat generation. Also, Jat and Chaudhary, in their analysis of MHD boundary layer flow over a uniformly stretching sheet with effects of porosity, thermal radiation and heat generation, Ohmic dissipation effect was not considered. Syed et al. (2012) presented parametric study of stagnation point hydromagnetics boundary layer flow over an axisymmetric permeable shrinking sheet with viscous dissipation and heat transfer in an expanse of an electrically conducting fluid ignoring the influence of thermal radiation and Ohmic dissipation. Of late, Ibrahim (2014) analyzed two-dimensional radiative MHD boundary layer flow of an incompressible, viscous and electrically conducting fluid caused by a non-isothermal linearly stretching sheet placed at the bottom of a fluid saturated with a porous medium in the presence of thermal radiation, viscous dissipation and homogeneous chemical reaction. Up to date, to the best awareness of the author, in the open literature the present problem of interest, motivated by the simultaneous neglect of thermal radiation, heat generation and Ohmic dissipation in boundary layer MHD flow of a viscous electrically conducting laminar flow over a permeable plate was not considered in spite of the practical importance in technological and industrial processes such as metallurgical production of metals and alloys in which the plate temperature is not isothermal, and transport processes around deep geological repositories for the disposal of high-level nuclear waste, for example the use of magnetic fields to curtail unwanted natural convection in the casting of aluminium, which are detrimental to the ingot structure, Davidson (2001).

2. Mathematical Analysis

Consider steady, laminar, boundary layer two-dimensional incompressible electrically conducting fluid occupying the upper porous half –space of (x, y)-plane, under the influence of a transversely imposed magnetic field $\boldsymbol{B}_0$ to a permeable rigid plate at y=o. The positive y-axis is taken normal to the plate while x-axis runs parallel to the plate, see Fig.1.

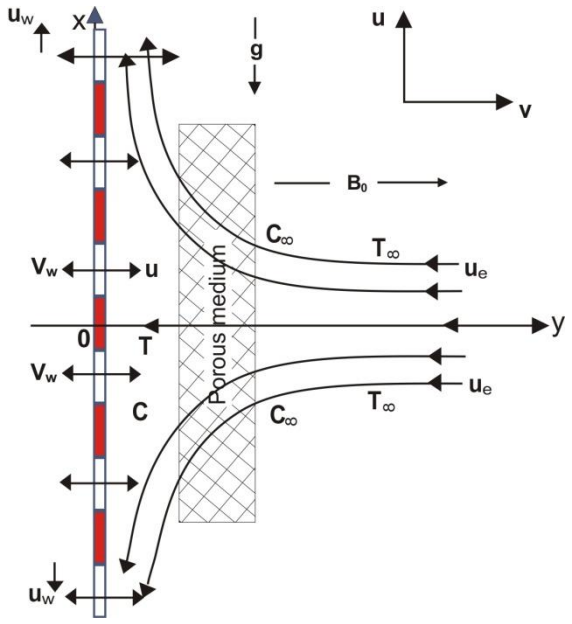

Fig. 1. Physical model and coordinate system

Two equal but opposite forces are applied along the parallel to the plate to initiate its stretching, keeping Origin, O the stagnation point of the flow fixed. The flow is partly induced into motion in effect to the plate stretching with a velocity $U_w = bx$ $(b > 0)$, which is proportional to distance x from O. Assuming that the magnetic Reynolds number is negligibly small in comparison with the imposed magnetic field, Sparrow and Cess (1978), the governing equations of flow, heat and mass transfer, taking into consideration of Boussinesq and boundary layer approximations are:

Governing Equations

$$\frac{\partial u}{\partial x} + \frac{\partial \mathrm{v}}{\partial y} = 0 \tag{1}$$

$$u\frac{\partial u}{\partial x} + \mathrm{v}\frac{\partial u}{\partial y} = -\frac{1}{\rho}\frac{\partial p}{\partial x} + \mathcal{V}\frac{\partial^2 u}{\partial y^2} + g\beta(\mathrm{T} - \mathrm{T}_\infty) + g\beta^*(C - C_\infty) - \frac{\sigma_e}{\rho}B_O(E_o + B_O\mathrm{u}) - \frac{\mathcal{V}}{K}u \tag{2}$$

$$0 = -\frac{1}{\rho}\frac{\partial p}{\partial y} \tag{3}$$

$$\mathrm{u}\frac{\partial \mathrm{T}}{\partial \mathrm{x}} + \mathrm{v}\frac{\partial \mathrm{T}}{\partial \mathrm{x}} = \frac{\mathrm{k}}{\rho \mathrm{C_p}}\frac{\partial^2 \mathrm{T}}{\partial \mathrm{y}^2} + \frac{\mathrm{Q}}{\rho \mathrm{C_p}}(\mathrm{T} - \mathrm{T}_\infty) + \frac{\sigma_e \mathrm{B_O^2}}{\rho \mathrm{C_p}}(\mathrm{u} - \mathrm{u_e})^2 - \frac{1}{\rho \mathrm{C_p}}\frac{\partial \mathrm{q_r}}{\partial \mathrm{y}} \tag{4}$$

$$\mathrm{u}\frac{\partial \mathrm{C}}{\partial \mathrm{x}} + \mathrm{v}\frac{\partial \mathrm{C}}{\partial \mathrm{x}} = \mathrm{D_m}\frac{\partial^2 C}{\partial y^2} - K_r(C - C_\infty)^n \tag{5}$$

Boundary Conditions:

$$\left.\begin{array}{lll} \mathrm{y} = 0: & u(x,0) = \sigma U_w\,,\ \mathrm{v}(x,0) = V_w\,, & T = T_W = cx + T_\infty, C = C_W = dx + C_\infty \\ & y \to \infty: \qquad u \to u_e\ , & T \to T_\infty,\quad C \to C_\infty \end{array}\right\} \tag{6}$$

and the transpiration (mass flux) velocity at the plate surface is V_w, with $V_w <$ 0 for suction or fluid withdrawal, $V_w > 0$ for injection or mass blowing, $V_w = 0$ corresponding to an impermeable plate. Further, u and v are the components of fluid velocity, $u_e = ax$ is the free stream speed (a is free stream speed constant and the arbitrary numbers $c, d \geq 0$), ρ the fluid density, σ_e is the electric conductivity, p is the fluid

pressure, $\mathcal{V}$ is the kinematic viscosity of the fluid, k is the thermal conductivity, c_P is the specific heat capacity at constant pressure, q_r is the radiative heat flux, K_r is the reaction rate constant, with $K_r > 0$ for destructive chemical reaction and $K_r < 0$ for generative chemical reaction, n is the order of homogeneous chemical reaction, T is the fluid temperature, C is the species concentration, T_W is the wall temperature of heated plate , C_W is the species concentration at the wall, T_∞ is the free stream temperature, C_∞ is the free stream species concentration, σ is the stretching/shrinking parameter, with $\sigma > 0$ for stretching and $\sigma < 0$ for shrinking, and Q is the volumetric rate of heat generation (source) /absorption (sink) , with $Q > 0$ for heat generation and $Q <0$ for heat absorption .

. In eqn. (2), allowance has been made for the possibility of an imposed electric field , $\boldsymbol{E}_o$ in the z-direction , whereby the corresponding Ohm's law which relates the electric current density **J** to the electric field and the fluid velocity **u** , and electromagnetic force $\boldsymbol{F_e}$ are (see Davidson, 2001):

$$J = \sigma_e(E_o + B_o u)\,, \qquad \boldsymbol{F_e} = \boldsymbol{J} \times \boldsymbol{B_o} = -\sigma_e B_o(E_o + B_o u) \tag{7}$$

Our model presumes that not only the stretching plate and free stream vary linearly in distance x from a fixed point located on the plate but also the wall temperature and the wall species concentration.

It may be mentioned here, that the fluid considered in this study shall be assumed to be thin (gray), emitting/absorbing radiation but not a scattering porous medium, Damseh et al. (2006). Also it is presumed that only the fluid can radiate thermally, and that account is made only for unidirectional heat flux perpendicular to the horizontal plates. Assumption is made of the local thermal equilibrium between porous matrix of the medium and the electrically conducting fluid. Taking into account of all stated premises above, use is made of Rosseland diffusion approximation to reduce the radiation term of eqn. (4) to that devoid of sacrificing appreciable accuracy within engineering context following Siegel and Howell (1972), the radiative heat flux is posited in the form:

$$q_r = -\frac{4\sigma^*}{3k^*}\frac{\partial T^4}{\partial y}\,, \tag{8}$$

where σ^* is the Steffan-Boltzman constant and k^* is the mean absorption coefficient.

Essentially, the use of Taylor's theorem for the expansion of temperature dependent function F(T) about the stream temperature T_∞, lends itself to the smallness of temperature difference $T - T_\infty$. Consequent upon which

$$\mathrm{F}(T) = F(T_\infty) + (T - T_\infty)F'(T_\infty) + \frac{1}{2!}(T - T_\infty)^2 F''(T_\infty) + \cdots \tag{9}$$

where prime signifies differentiation with respect to T.

On replacing F(T) by T^4 in eqn. (9), neglecting higher order terms , one obtains

$$T^4 \approx T_\infty^3(4T - 3T_\infty)\,.$$

Using this discerningly in eqn. (8) , we find

$$q_r = -\frac{16\sigma^* T_\infty^3}{3k^*}\frac{\partial T}{\partial y} \quad , \quad \frac{\partial q_r}{\partial y} = -\frac{16\sigma^* T_\infty^3}{3k^*}\frac{\partial^2 T}{\partial y^2} \tag{10}$$

Outside the boundary layer, in the far field the boundary layer solution must be matched to the inviscid flow solution, where

$$y \to \infty,\ u \to u_e\ ,\ p \to p_\infty\ ,\ \rho \to \rho_\infty\ ,\ T \to T_\infty \tag{11}$$

Substituting the boundary conditions (11) into eqn. (2), one obtains (see Shivamoggi , 1985)

$$u_e \frac{du_e}{dx} = -\frac{1}{\rho_\infty}\frac{dp_\infty}{dx} - \frac{\sigma_e}{\rho}B_o(E_o + B_o u) - \frac{\nu}{K}u_e \tag{12}$$

It is self indicating from eqn. (3) that $p = p(x)$ only. Eliminating $\frac{dp_\infty}{dx}$ between eqns. (2) and (12), dropping subscript ∞ , we obtain

$$u\frac{\partial u}{\partial x} + \mathrm{v}\ \frac{\partial u}{\partial y} = u_e \frac{du_e}{dx} + \nu\frac{\partial^2 u}{\partial y^2} + g\beta(\mathrm{T} - \mathrm{T}_\infty) + g\beta^*(C - C_\infty) - \frac{\sigma_e}{\rho}{B_0}^2(u - u_e) - \frac{\nu}{K}(u - u_e) \tag{13}$$

Convincingly, the electric field has no contributing influence on the MHD boundary layer equations as seen in eqn.(13).

Substituting (9) – (11) into (4), we obtain

$$u\frac{\partial T}{\partial x} + \mathrm{v}\frac{\partial T}{\partial x} = \frac{k}{\rho c_P}\left(1 + \frac{16\sigma^*}{kk^*}\right)\frac{\partial^2 T}{\partial y^2} + \frac{Q}{\rho c_P}(T - T_\infty) + \frac{\sigma_e B_O^2}{\rho c_P}(u - u_e)^2 \tag{14}$$

3. Method of solution

In order that continuity equation (1) be satisfied, the stream function $\psi(x, y)$ is introduced such that the velocity components u, v are defined by

$$u = \frac{\partial \psi}{\partial y}\ ,\ \ \mathrm{v} = -\frac{\partial \psi}{\partial x} \tag{15}$$

Appropriate similarity transformation for this present problem is the set of the following expressions

$$\eta = y\sqrt{\frac{b}{\nu}},\ \psi(x, y) = x\sqrt{\nu b}f(\eta),\ \theta(\eta) = \frac{T - T_\infty}{T_w - T_\infty},\quad \phi(\eta) = \frac{C - C_\infty}{C_w - C_\infty} \tag{16}$$

where η is the similarity variable, $f(\eta)$is the dimensionless stream function and the non-dimensional temperature and species concentration fields are $\theta(\eta)$ and $\phi(\eta)$ respectively.

By substituting (15) and (16) into the momentum, energy and species concentration equations (2)− (5), and also boundary conditions (6) , one obtains the following nonlinear coupled ordinary differential equations:

$$f''' + ff'' - (f')^2 + Gr\theta + Gc\phi - (M + A)(f' - \varepsilon) + \varepsilon^2 = 0 \tag{17}$$

$$\left(1 + \frac{4}{3}Ra\right)\theta'' + Prf\theta' - Prf'\theta + PrS\theta + PrEcM(f' - \varepsilon)^2 = 0 \tag{18}$$

$$\phi'' + Scf\phi' - Scf'\phi - ScK\phi^n = 0 \tag{19}$$

together with the transformed boundary conditions:

$$\left.\begin{aligned} &\eta = 0\text{:}\ f(\eta) = Fw,\ f'(\eta) = \sigma\ ,\ \ \theta(\eta) = 1,\ \ \phi(\eta) = 1 \\ &\eta \to \infty :\ \ f'(\eta) \to \varepsilon\ ,\ \ \theta(\eta) \to 0,\ \ \phi(\eta) \to 0 \end{aligned}\right\} \tag{20}$$

where prime denotes differentiation with respect to η.

The existence of similarity solutions demands that V_w be of the form (Yian et al., 2011; Adeniyan and Ogwuegbu, 2014)

$$V_w = -\sqrt{b\mathcal{V}}\, F_w \tag{21}$$

where $F_w = f(0)$, with $F_w > 0$ *and* $F_w < 0$ respectively stand for mass suction (or mass withdrawal) and mass injection (or mass blowing). The dimensionless quantities involved in this boundary layer problem, nomenclature-wise are the suction/injection parameter F_w, the Prandtl number Pr, the magnetic parameter M, the porous medium permeability parameter A, the velocity ratio parameter ε, the Eckert number Ec, the heat generation or absorption parameter S, the thermal radiation parameter Ra, the Schmidt number Sc, the chemical reaction rate parameter K, the respective modified thermal and solutal Grashof numbers Gr and Gc. These parameters are as given:

$$\left.\begin{aligned} F_w = -\frac{V_w}{\sqrt{\mathcal{V}b}}, \quad Pr = \frac{\mathcal{V}}{\alpha}, \quad M = \frac{\sigma_e B_0^2}{\rho b}, \quad A = \frac{\mathcal{V}}{Kb}, \\ \varepsilon = \frac{a}{b}, \quad Ec = \frac{U_w^2}{C_p(T_{W-T\infty})}, \quad S = \frac{Q_0}{b\rho C_p}, \quad Ra = 4\frac{\sigma^* T_\infty^3}{kk^*}, \\ Sc = \frac{\mathcal{V}}{\mathrm{D_m}}, \quad K = \frac{K_r}{b}[(C_w - C_\infty)\phi]^{n-1}, \quad Gr = \frac{g\beta(T_{W-T\infty})x}{U_w^2}, \quad Gc = \frac{g\beta^{*(C_W-C\infty)}x}{U_w^2} \end{aligned}\right\} \tag{22}$$

It is worth noting that in practice n, the order of homogeneous chemical reaction takes on the values $n = 1, 2, 3$ for meaningful practical situation. Also K<0 and K>0 respectively demonstrate generative and destructive chemical reactions.

4. Skin-Friction, Heat and Mass Transfer Coefficients

Some pertinent flow, heat and mass transfer characteristics in this study include the local skin friction coefficient C_{fx}, the local Nusselt number Nu_x , and the local Sherwood number Sh_x posited respectively as

$$u = bf'(\eta), \quad \mathrm{v} = -\sqrt{\mathcal{V}b}f(\eta) \tag{23}$$

$$C_{fx} = \frac{\tau_w}{\rho u_\infty^2}\ , \quad Nu_x = \frac{xq_w(x)}{k(T_{W-T\infty})}\ , \quad Sh_x = \frac{xq_m(x)}{\mathrm{D_{m(}}_{C_W-C\infty)}}\ , \tag{24}$$

where τ_w the wall shear stress, q_w the wall surface heat flux and q_m the wall surface mass flux are

$$\tau_w = \rho\mathcal{V}\left(\frac{\partial u}{\partial y} + \frac{\partial v}{\partial x}\right)(x,0)\,, q_w = -k\left(1 + \frac{4}{3}Ra\right)\frac{\partial T}{\partial y}(x,0), q_m = -\mathrm{D_m}\frac{\partial C}{\partial y}(x,0) \tag{25}$$

In terms of the local Reynolds number $Re_x = \frac{x\,u_w}{\mathcal{V}}$, the reduced forms of physical quantities of importance are

$$C_f Re_x^{\frac{1}{2}} = f''(0), \ \ Nu_x Re_x^{-\frac{1}{2}} = -\left(1 + \frac{4}{3}Ra\right)\theta'(0), \ \ Sh_x Re_x^{-\frac{1}{2}} = -\phi'(0) \tag{26}$$

5. Numerical Simulation

The set of highly nonlinear coupled 3rd and 2nd order ordinary differential equations (17) – (19) subject to the boundary conditions (20) constitutes two-point boundary value problems (BVPs). In order to tackle these equations numerically using Runge-Kutta-Fehlberg integration scheme, one often needs first and foremost, to convert the BVPs into a system of initial value problems (IVPs). The procedural steps of which are itemized in the published papers of Ibrahim and Makinde (2010, 2011), Makinde(2011), Mukhopadhyay (2012, 2013), among others Another issue of challenge crucial to this scheme is the appropriate choice of finite values of η as $\eta \to \infty$. The scheme involves the discretization of the problem domain $0 \leq \eta \leq \boldsymbol{\eta_{max}}$, where $\boldsymbol{\eta_{max}}$ is a large finite value selected by trial-and-error which conveniently replaces $\eta \to \infty$. It is important to notice that these present problem equations as IVPs, involve 7 first order simultaneous equations and in order to proffer solutions for them using the scheme, one requires seven in initial conditions as against the prescribed four, namely $f(0), f'(0)$on $f(\eta)$, $\theta(0)$on $\theta(\eta)$ and $\phi(0) on\ \phi(\eta)$. However, the 3 unspecified conditions $f''(0)$ on $f(\eta), \theta'(0)$on $\theta(\eta)$and $\phi'(0)$on $\phi(\eta)$ with assigned guesses, are then evaluated using the asymptotic values $f'(\boldsymbol{\eta_{max}}) = \mathcal{E}, \theta(\boldsymbol{\eta_{max}}) = 0$ and $\phi(\boldsymbol{\eta_{max}}) = 0$, by means of an efficient shooting technique alongside the integration scheme. Further yet-to resolve issue of challenge is minimization of errors in the guessed values of the un-prescribed initial conditions up to the desired significant accuracy. However, the last challenging issue is addressed using selected value of $\boldsymbol{\eta_{max}}$ along with the guessed initial boundary conditions, and then carry out the numerical integration using the Runge-Kutta-Fehlberg integration scheme. The process is repeated for each $\boldsymbol{\eta_{max}}$ such that differences between two successive values of $f''(0)$, $\theta'(0)$ and $those\ of\ \phi'(0)$ are less than 10^{-7} with step size $\Delta\eta = 0.001$ to obtain the numerical solution with a seven decimal place accuracy as criterion for convergence in nearly all cases considered and $\boldsymbol{\eta_{max}} = 10$. The executions of solution were implemented on a computer program that uses the symbolic and computational language, in Maple (Heck, 2003). It is now a general perception that nonlinear system of differential equations alongside the appropriate boundary conditions for a well-posed problem may admit more than one solution, provided that each of the solutions is stable (Merkin, 1985; Ridha, 1996; Makinde and Olanrewaju, 2012).

6. Results and Discussion

6.1 Tabular Results

As explained in the preceding paragraph, the analysis for the computations has been carried out by means of the processes therein for various basic flow parameters, namely :

thermal Grashof number Gr, solute Grashof number Gc, Prandtl number Pr, Eckert number Ec, Schmidt number Sc, thermal radiation parameter Ra, Suction/injection parameter Fw, Magnetic parameter M, porous medium permeability parameter A, chemical reaction rate parameter K, the heat generation or absorption parameter S, velocity ratio ε, and stretching/shrinking parameter σ. This parametric study has been carried out adopting the following values $Gr = Gc = Pr = Sc = Ec = Ra = M = A = K = S = \sigma = \varepsilon = 0.1$, $Fw = 0.5$ and $n = 1$ for the basic flow parameters. Thusly, situation in which each parameter adjusts values, in the tables has been appropriately highlighted therein, and on the graphs depicted specifically on the figure legends. Tables 1 and 2 depict the comparison of Ishak et al. (2007) reported results as special cases of the present work, therefore indicating favorable agreement and our numerical code is adduced credible. The crux of this present work is centered on cooling problems with applications in engineering and related areas, the relevant situations are those for which the buoyancy force parameters $(Gr, Gc)$are nonenegative. Tables 3-4 present the variations in the reduced local skin friction coefficient $C_f Re_x^{\frac{1}{2}} = f''(0)$, reduced local Nusselt number $Nu_x Re_x^{-\frac{1}{2}} = -\left(1 + \frac{4}{3}Ra\right)\theta'(0)$ and reduced local Sherwood number $Sh_x Re_x^{-\frac{1}{2}} = -\phi'(0)$ for various values of emerging flow controlling parameters. In each of the considered situation the varying parameter has been highlighted while others maintained their fixed given values. As observed, increase in the buoyancy forces (Gr, Gc), the thermal conductivity and radiation $(\mathcal{E}, Ra)$, chemical reaction order (n), suction (Fw>0) and stretching $(\sigma > 0)$ parameters leads to an increase in the reduced local skin friction coefficient, local Nusselt and Sherwood numbers whereas increase in drag-like forces (M, A), suction (Fw<0) and shrinking $(\sigma < 0)$ parameters produces reverse effect. However, increase in Schmidt number (Sc) and destructive chemical reaction parameter (K>0) gives rise to decreasing values of the reduced local skin friction and local Nusselt number while the opposite trend has been observed for the reduced local Sherwood number. As recoded in these tables, the reduced local Sherwood number can be decreased by an increase in either of the Prandtl number (Pr), heat energy absorption (S<0) and chemical reaction generative (K<0) parameters but opposite effects are revealed on the reduced local Nusselt number. Increase in the Prandtl number and heat absorption parameter results into a decrease in the reduced local skin friction coefficient. However the influence of the increase in the Pr and heat energy absorption (S<0) produces an increase in the reduced local Nusselt number.

Table 1: Computations showing comparison of the Nusselt number with Ishak et al.[2007] result when $Pr = 1,\ 10,\ \sigma = 1,\ Gr = Gc = Sc = Ra = \mathcal{E} = 0$

Flow parameters With fixed values	Fw	Ishak et al.[2007]	Present study
		$Nu_x Re_x^{-\frac{1}{2}}$	$Nu_x Re_x^{-\frac{1}{2}}$
Pr=1	-1	0.6181	0.6182
	-0.6	0.7441	0.7441
	-0.4	0.8198	0.8199
	-0.2	0.9050	0.9050
	0	1.0000	1.0000
	0.2	1.1050	1.1050
	0.4	1.2198	1.2198
	0.6	1.3440	1.3440
	1	1.6180	1.6180
Pr=10	-1	0.9418	0.9417
	-0.6	1.4709	1.4708
	-0.4	1.9681	1.9679
	-0.2	2.7096	2.7094
	0	3.7208	3.7207
	0.2	4.9765	4.9763
	0.4	6.4260	6.4258
	0.6	8.0178	8.0177
	1	11.4762	11.4760

Table 2: Computations showing comparison of the Skin-friction coefficient and the Nusselt number with Ishak et al. [2007] results when Pr=1, $\sigma = 1, Gr = 0, -0.1, 1$ while $Gc = Sc = Ra = Fw = 0$.

Flow parameters With fixed values	ε	Ishak et el.[2007]		Present result	
		$C_f Re_x^{\frac{1}{2}}$	$Nu_x Re_x^{-\frac{1}{2}}$	$C_f Re_x^{\frac{1}{2}}$	$C_f Re_x^{\frac{1}{2}}$
Pr=1, Gr=0	0	-0.9980		-0.9985	
	0.1	-0.9694		-0.9694	
	0.2	-0.9181		-0.9181	
	0.5	-0.6673		-0.6673	
	2	2.0175		2.0178	
	3	4.7294		4.7843	
	10	36.2603		36.5751	
Pr=1, $Gr = -0.1$,	0	-1.0513	0.9856	-1.0514	0.98558
	0.01	-1.0490	0.9880	-1.0490	0.987943
	0.05	-1.0372	0.9977	-1.0372	0.997694
	0.1	-1.0176	1.0079	-1.0176	1.010402
	0.2	-0.9638	1.0362	-0.9638	1.036868
	0.5	-0.7075	1.1186	-0.7075	1.118574
	1	-0.0343	1.2502	-0.0343	1.250185
	2	1.9899	1.4855	1.9899	1.485551
	5	11.7331	2.0418	11.7609	2.064926
Pr=Gr=1	0	-0.5608	1.0873	-0.56092	1.087214
	0.01	-0.5596	1.0881	-0.5597	1.088082
	0.05	-0.5528	1.0921	-0.55772	1.091849
	0.1	-0.5398	1.0982	-0.5398	1.098245
	0.2	-0.5002	1.1133	-0.50018	1.113302
	0.5	-0.2846	1.1714	-0.28458	1.171363
	1	0.3350	1.2827	0.334974	1.282694
	2	2.2913	1.5020	2.291024	1.503357
	5	11.9449	2.0473	11.96833	2.06992

Table 3: Computations showing the reduced Skin-friction coefficient $C_f Re_x^{\frac{1}{2}}$, reduced Nusselt number $Nu_x Re_x^{-\frac{1}{2}}$, reduced Sharwood number $Sh_x Re_x^{-\frac{1}{2}}$ for various indicated basic flow parameter values

Gr	Gc	M	A	ε	Ra	Pr	$C_f Re_x^{\frac{1}{2}}$	$Nu_x Re_x^{-\frac{1}{2}}$	$Sh_x Re_x^{-\frac{1}{2}}$
0.1	0.1	0.1	0.1	0.1	0.1	0.1	0.22123234	0.18185328	0.21477423
0.5	0.1	0.1	0.1	0.1	0.1	0.1	0.57780253	0.23250561	0.25712265
1	0.1	0.1	0.1	0.1	0.1	0.1	0.95494809	0.27029372	0.28953073
0.1	0.5	0.1	0.1	0.1	0.1	0.1	0.56399608	0.22794047	0.25350029
0.1	1	0.1	0.1	0.1	0.1	0.1	0.93097531	0.26371231	0.28424654
0.1	0.1	0.5	0.1	0.1	0.1	0.1	0.17644858	0.16768096	0.28063631
0.1	0.1	1	0.1	0.1	0.1	0.1	0.14860436	0.15955364	0.27057234
0.1	0.1	0.1	0.5	0.1	0.1	0.1	0.17644093	0.16778484	0.28063229
0.1	0.1	0.1	1	0.1	0.1	0.1	0.14859717	0.15968904	0.27056830
0.1	0.1	0.1	0.5	0.5	0.1	0.1	0.58566811	0.26358606	0.27950469
0.1	0.1	0.1	0.5	1	0.1	0.1	1.36567133	0.35629314	0.35770526
0.1	0.1	0.1	0.5	0.1	0.5	0.1	0.22352904	0.23800556	0.21566338
0.1	0.1	0.1	0.5	0.1	1	0.1	0.22503389	0.30655625	0.21625127
0.1	0.1	0.1	0.5	0.1	0.1	0.72	0.19758661	0.42059467	0.20667282
0.1	0.1	0.1	0.5	0.1	0.1	1	0.19225578	0.48947866	0.20524493
0.1	0.1	0.1	0.5	0.1	0.1	2	0.18074852	0.67458077	0.20271946

Table 4: Computations showing the reduced Skin-friction coefficient $C_f Re_x^{\frac{1}{2}}$, reduced Nusselt number $Nu_x Re_x^{-\frac{1}{2}}$, reduced Sharwood number $Sh_x Re_x^{-\frac{1}{2}}$ for various indicated basic flow parameter values

S	Ec	Sc	K	n	σ	Fw	$C_f Re_x^{\frac{1}{2}}$	$Nu_x Re_x^{-\frac{1}{2}}$	$Sh_x Re_x^{-\frac{1}{2}}$
-0.3	0.1	0.1	0.1	1	0.1	0.5	0.21373573	0.27022227	0.21226769
-0.1	0.1	0.1	0.1	1	0.1	0.5	0.21714528	0.22898940	0.21339515
0	0.1	0.1	0.1	1	0.1	0.5	0.21908982	0.20628260	0.21404804
0.1	0.1	0.1	0.1	1	0.1	0.5	0.22123234	0.18185328	0.21477423
0.3	0.1	0.1	0.1	1	0.1	0.5	0.22627264	0.12641837	0.21650400
0.1	0.1	0.5	0.1	1	0.1	0.5	0.19957869	0.17335696	0.45374302
0.1	0.1	1	0.1	1	0.1	0.5	0.18835049	0.17025387	0.63211889
0.1	0.1	0.1	-0.2	1	0.1	0.5	0.22801161	0.18470508	0.14410429
0.1	0.1	0.1	-0.1	1	0.1	0.5	0.22549781	0.18363579	0.16966050
0.1	0.1	0.1	0.1	1	0.1	0.5	0.22123234	0.18185328	0.21477423
0.1	0.1	0.1	0.5	1	0.1	0.5	0.21475065	0.17925126	0.28877911
0.1	0.1	0.1	1	1	0.1	0.5	0.20890740	0.17705433	0.36305470
0.1	0.1	0.1	0.1	1	0.1	0.5	0.22123234	0.18185328	0.21477423
0.1	0.1	0.1	0.1	2	0.1	0.5	0.22210407	0.18227901	0.20805899
0.1	0.1	0.1	0.1	1	-0.2	0.5	0.36774657	0.13293394	0.16855000
0.1	0.1	0.1	0.1	1	-0.1	0.5	0.33937739	0.15151678	0.18595057
0.1	0.1	0.1	0.1	1	0	0.5	0.28985796	0.16757780	0.20115041
0.1	0.1	0.1	0.1	1	0.1	0.5	0.22123234	0.18185328	0.21477423
0.1	0.1	0.1	0.1	1	1	0.5	-1.10243183	0.27322498	0.30388071
0.1	0.1	0.1	0.1	1	0.1	-3	0.19007226	0.16447138	0.19702072
0.1	0.1	0.1	0.1	1	0.1	-5	0.17317007	0.15476835	0.18712299
0.1	0.1	0.1	0.1	1	0.1	0	0.21672334	0.17933745	0.21220433
0.1	0.1	0.1	0.1	1	0.1	3	0.24364437	0.19461655	0.22780335
0.1	0.1	0.1	0.1	1	0.1	5	0.26100524	0.20507703	0.23846203

6.2. Graphical Results

5.2.1. Effect of parametric variation on velocity Velocity field

Figs. (2) – (10) present the trend of the velocity profiles for various values of the basic flow parameters considered in Tables 4-5 of our computational results. Fig. 2 demonstrates the variation of the velocity profiles $f(\eta)$ with the spanwise distance η for increasing

thermal Grashof numbers (Gr) from 0.1 through 1.0. The velocity rises markedly from the surface wall value with a very sharp overshot near the wall afterwhich it nozedives fastly to assume the asymptotic far field value. The variations of the velocity with respect to the solutal Grashof number featured similar trend to those of the Gr, they had been omitted for brievity. The effect of variation of the velocity with the magnetic field parameter (M) is depicted in Fig. 3 where the velocity starts with the wall value of $\sigma = 0.1$ and rises to attain a peak value near the wall, thereafter a rapid fall in the fluid velocity occurs as M increases from 0.1 through 1.0. The results recorded for the influence of the variations of the permeability parameter of the porous medium (A) for the same range of variation and those due to the Prandtl number (Pr) in the range 0.72 through 2.0 along with the Shimdt number (Sc) in the range $0 < Sc \leq 1$ were omitted in this report as their trends were not different from those of Fig. 3. Increasing the magnetic field strength gives rise to increased interaction between the fluid motion and the transverse magnetic field permeating the fluid which in consequence promotes enhancement of the magnitude of the Lorentz force which opposes the buoyancy forces resulting into inhibition of the fluid velocity. In a similar fasion, the Darcy force whose existence is based on the porous marix material in the flow impeds the fluid velocity as it grew in srenhth, this again had been omitted in this report for brevity. Fig. 4 shows the velocity profiles for the velocity ratio parameter. As shown, the fluid velocity rises in the boundary layer from the wall value of 0.1 to attain the asymptotic free stream value . Increase in the velocity ratio leads to a rise in the fluid velocity profiles. Figs. 5 and 8 depict the velocity profiles for various values of the radiation parameter Ra ($0 \leq Ra \leq 1$) and chemical reaction order parameter n, where in practice ($n = 1, 2$)while the case for 3rd order reaction is sparse. As it can be seen, the fluid velocity increases with increase in Ra, but mildly increases with increasing chemical reaction order n. The variation of the velocity field $f(\eta)$ with with spanwise distance η for various values of heat generation/absurption parameter has been signposted in Fig. 6. As observed, the velocity rises with increasing internal heat generation parameter (S>0) and falls with rise in the heat absurption parameter (S<0). Also as featured in Fig. 7 for chemical reaction parameter (K) in the interval range $[-0.2, 1]$, the velocity rises as the generative chemical reaction parameter (K<0) intensifies in values, but the reverse is the case as the destructive chemical reaction parameter (K>0) increases in values. Fig. 9 unveils the variation in the velocity profiles as the stretching/shrinking parameter ranges from -0.2 through 1.0. The trend reveals that the dimensionless velocity increases with increase in the stretching parameter ($\sigma > 0$) while opposite trend is demonstrated for increasing shrinking parameter ($\sigma < 0$). In Fig. 10, the velocity profiles increase with increase in the

injection parameter (Fw<0), but reduces with rise in suction parameter (Fw>0). It may be mentioned here that the physical phenomenon characterized by suction may be useful for putting into practice in technological and industrial processes where fluid velocity needs to be stemmed as to delay the boudary layer transition.

6.2.2. Effect of parametric variation on Temperature Field

The plots of the dimensionless temperature distribution against the the transverse distance for several emerging flow parameters are illustrated in Figs. $11-15$ wherein the distribution assumes the wall surface value of unity and subsequently decreases monotonically to admit its zero farfield value asymptotically. As it can be observed in Fig. 11, the fluid temperature within the boundary layer cools down considerably on raising the thermal Grashof number from 0.1 through 1.0. The same feature prevailed for increasing Solutal Grashof numbers (not reported here for space economy). Interstingly, this physical phenomenon has practical importace in some engineering problems where the fluid temperature in the thermal boundary layer demands control. Fig. 12 unveils the features of the variation of the magnetic field parameter (M) on the fluid dimensionless temperature field. An observable increase in temperature occurs when M strengthens from 0.1 through 1.0. A similar report was recorded when the solutal Grashof number was adjusted in the same range (not shown). The variation of temperation field $\theta(\eta)$ with respect to η is signposted in Fig. 13 wherein the fluid temperature within the boundary layer deminishes rapidly in values as the Prandtl number (Pr) increases from 0.72 (air) through 1.0 (geothermal water) to 2.0 (low temperature aquifer). The effects of heat generation/absurption on thermal profiles as observed in Fig. 14 shows that the fluid temperature can be raised by inceasing the heat generation parameter (S>0) while reverse trend manifests for the heat absurption parameter (S<0). Fig. 15 depicts the plots of the temperature field $\theta(\eta)$ versus η for various values of the stretching /shrinking parameter σ in interval $(-0.2, 1.0)$. The revelation lends to a rise in fluid temperature when shrinking parameter strengthens in values. On the other hand, there occurs a fall in temperature as the stretching parameter increases in values. From the other results not reported here for space saving, the effects of the suction or fluid withrawal dampened the thermal temperature and those of the injection or mass blowing raised it.

6.2.3. Effect of parametric variation on Concentration Field

Figs. $16-21$ addresses the variations of the dimensionless species concentration profles with various basic flow parameters. Again as in the cases of earlier section 5.2.2, each of the curves satisfactorily adheres to the wall and farfield boundary conditions. Fig. 16 shows the variation of of species concentration $\phi(\eta)$ with respect spanwise distance η for several

values of the Grashof number (Gr). As Gr increases from 0.1 to 1.0, a decrease in $\phi(\eta)$ occurs. This same feature, though omitted, was recorded for the variations accompanied by increase in the solutal Grashof number. Fig. 17 shows that the concentration profiles rise with increasing magnitude of the magnetic field parameter (M) and similar trend was observed when the porous medium permeability parameter (A) increases within the boundary layer (omitted). Fig. 18 depicts the variation of the species concentration profiles for varying Scmidt number (Sc). As it can be seen, the species concentration decreases in values as the Scmidt number increases. The effect of the velocity ratio ($\mathcal{E}$) was exacly similar in trend to those revealed by the Schmidt number, and subsequently omitted. The variation of dimensionless concentration $\phi(\eta)$ in the boundary layer as the chemical reaction parameter ranges from -0.2 through 1.0 is unveiled Fig. 19, wherein $\phi(\eta)$ rises with incresing generative chemical reaction parameter (K<0) in contrast with that of the destructive chemical reaction parameter (K>0). Figs. 20-21chacterize the effects of the shrinking/stretching and injection/suction parameters on the dimensionless species concentration respectively. As observed, both the shrinking and injection parameters cause a rise in the concentration whereas the stretching and suction parameter indicate the reverse trend.

6.2.4. Effect of parametric variation on the local skin friction, reduced local Nusselt and Sherwood numbers

The effects of Eckert number on the reduced local Nusselt number or local heat transfer $-\theta'(0)$ and reduced local Sherwood number or local mass transfer $-\phi'(0)$ are provided in Figs. 22 - 23 respectively for selected governing flow parameters. As observed, the local Sherwood number falls in magnitudes when the magnetic field parameter (M) rises for the curves of $\phi'(0)$ versus Ec in Fig. 23 and the same trend of response featured for the case of variation of the local skin friction coefficient or local wall shear stress parameter $f''(0)$ with Ec as M rose in values, though not presented here. However, Fig. 22 which depicts the variation of the reduced Nusselt number with the Eckert number, reveals that the local Nusselt number increases markedly with rising magnetic field parameter. From other results not presented in this report, the porous medium permeability parameter (A) caused a rise in the reduced local Nusselt number.

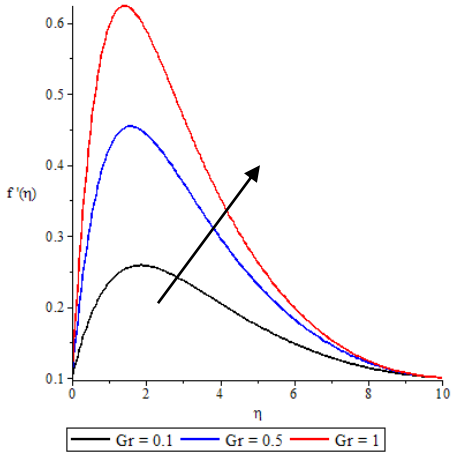

Fig. 2: Vellocity profile f' for various values of thermal Grashof number Gr

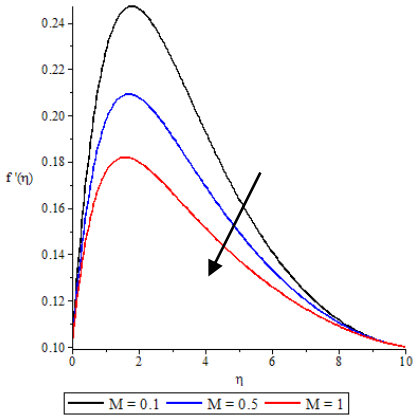

Fig. 3: Vellocity profile f' for various values Of Magnetic parameter M

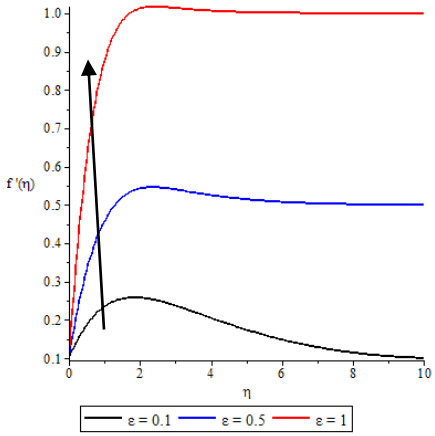

Fig. 4: Vellocity profile f' for various values of Velocity ratio parameter $\mathcal{E}$

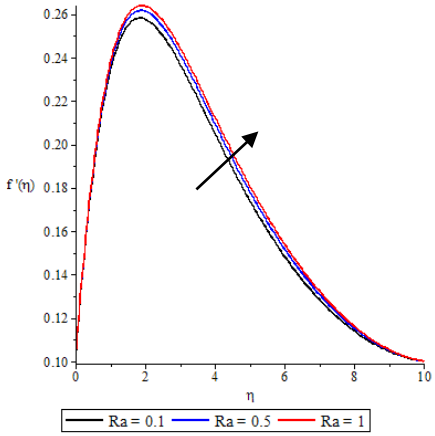

Fig. 5: Vellocity profile f' for various values of Radiation parameter Ra

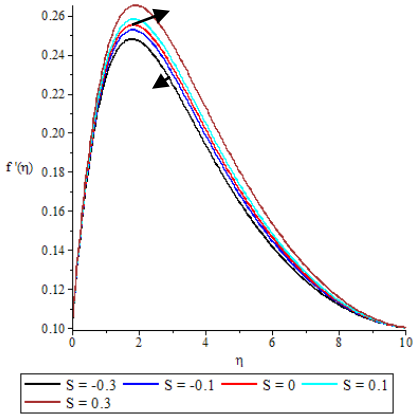

Fig. 6: Vellocity profile f' for various values of heat generation parameter S

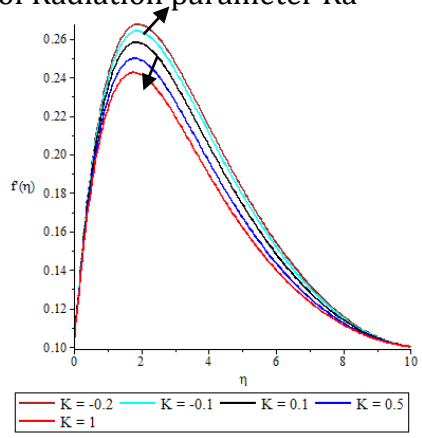

Fig. 7: Vellocity profile f' for various values of Chemical reaction parameter K

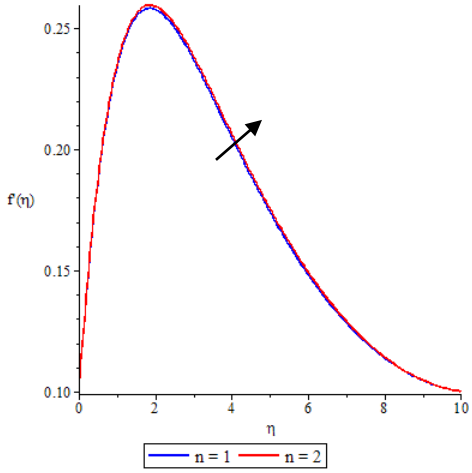

Fig. 8: Vellocity profile f' for various values of chemical reaction order n

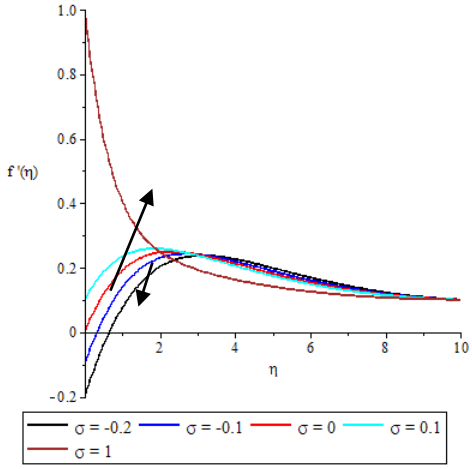

Fig. 9: Vellocity profile f' for various values of strething parameter σ

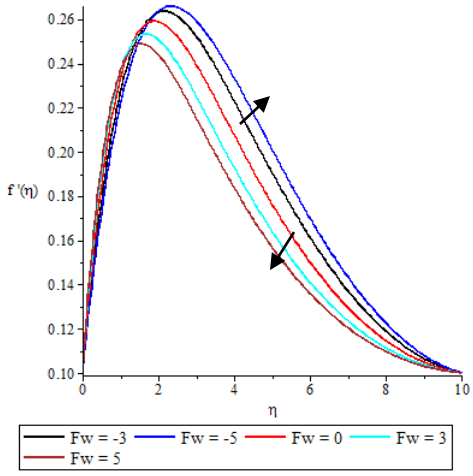

Fig. 10: Vellocity profile f' for various values of strething parameter Fw

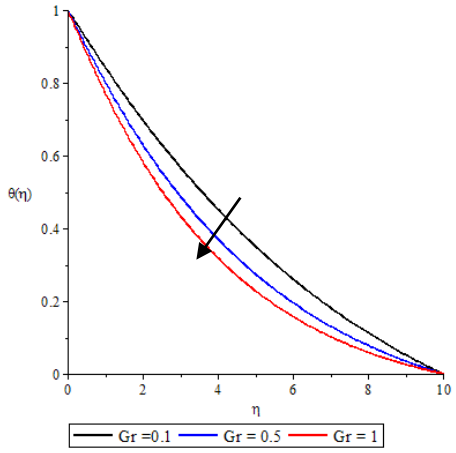

Fig. 11: Temperature profile θ for various values of thermal Grashof number Gr

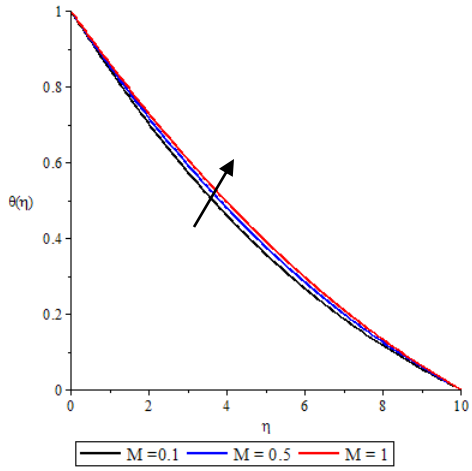

Fig. 12: Temperature profile θ for various values of magnetic parameter M

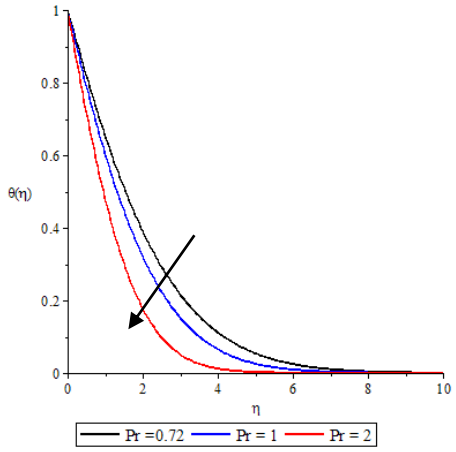

Fig. 13: Temperature profile θ for various values of Prandtl number Pr

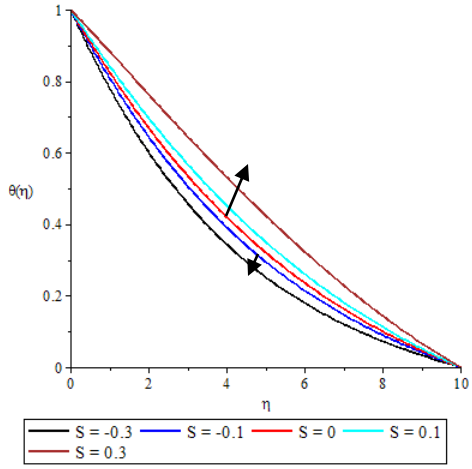

Fig. 14: Temperature profile θ for various values of heat generation /absorption parameter S

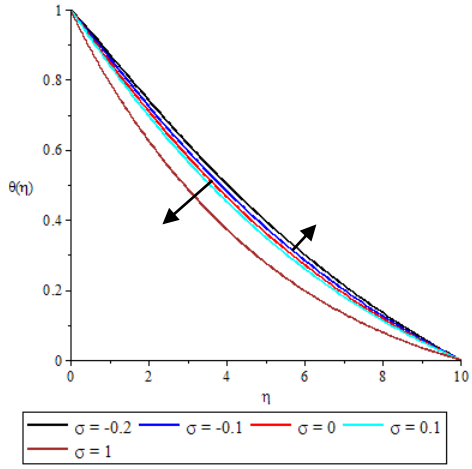

Fig. 15: Temperature profile θ for various values of stretching parameter σ

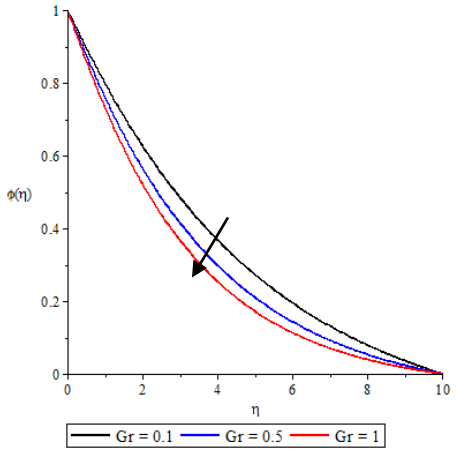

Fig. 16: Concentration profile ϕ for various values of stretching parameter Gr

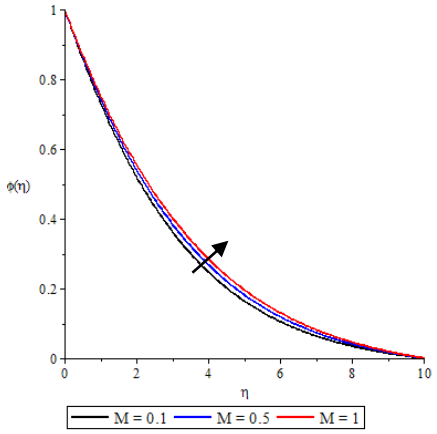

Fig. 17: Concentration profile ϕ for various values of stretching parameter M

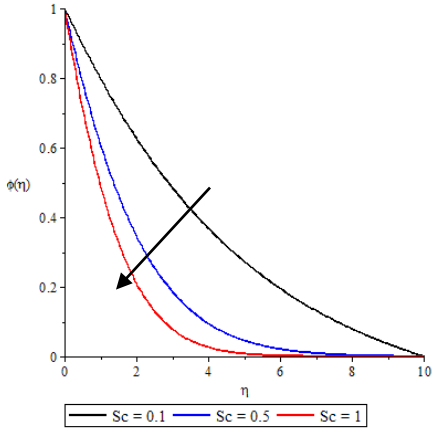

Fig. 18: Concentration profile ϕ for various values of stretching parameter S

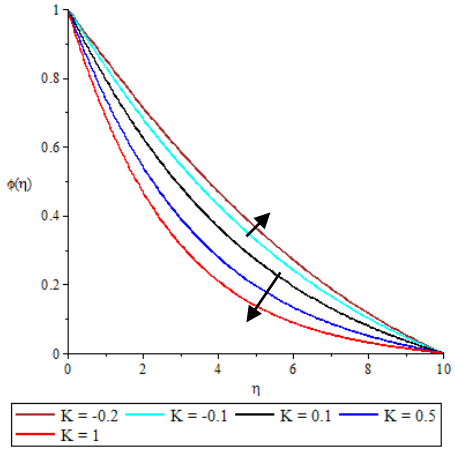

Fig. 19: Concentration profile ϕ for various values of stretching parameter K

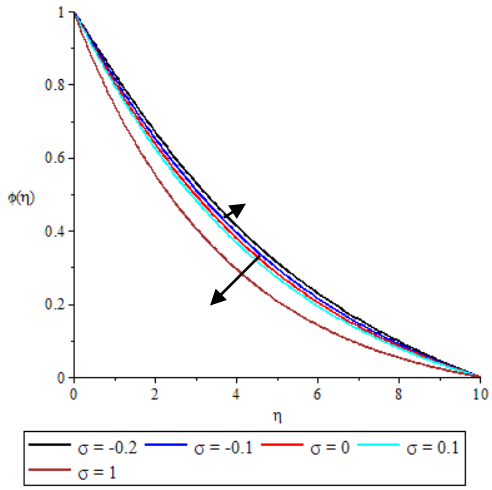

Fig. 20: Concentration profile ϕ for various values of stretching parameter σ

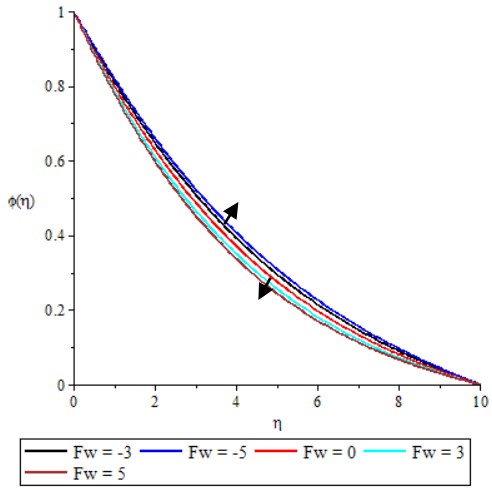

Fig. 21: Concentration profile ϕ for various values of stretching parameter F

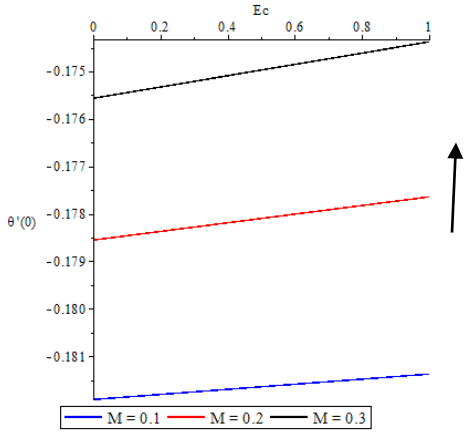

Fig. 22 : Variation of reduced Sherwood number $Sh_x Re^{-\frac{1}{2}} = \phi'(0)$ With Eckert number Ec for various of Magnetic parameter M

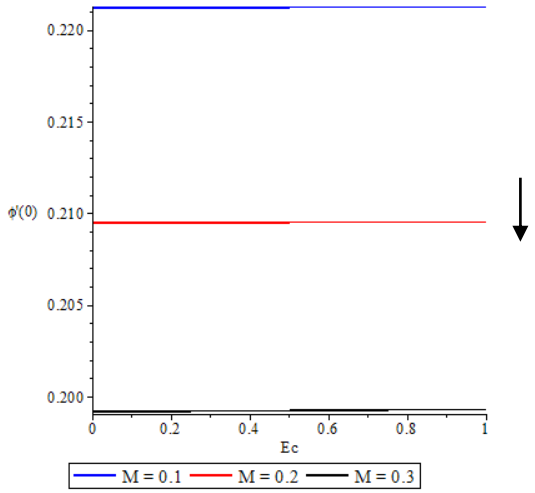

Fig. 23: Variation of reduced Sherwood number $Sh_x Re^{-\frac{1}{2}} = \phi'(0)$ With Eckert number Ec for various values of Magnetic parameter M

7. Conclusions

A similarity analysis has been carried out to investigate the influences on the steady, laminar boundary layer flow of the magnetoconvection heat and mass transfer near the vertical permeable plate encompassed in an electrically conducting fluid, stretching or shrinking linearly with respect to the axial distance and permeated by a uniform transverse magnetic field in the presence of uniform porous medium permeability, nth order chemical reaction and Joule heating. A linear assumption in the variation of the fluid temperature and species concentration with respect to the axial distance has been adduced. The results of our numerical findings are thus summarized:

- The local skin friction, the reduced local Nusselt and Sherwood numbers all increase in values as the buoyancy parameters (Gr, Gc), radiation (Ra), velocity ratio ($\mathcal{E}$), chemical reaction order (n), suction (Fw>0) and stretching ($\sigma > 0$) intensify, in contrast to increase in the magnetic field (M), permeability`(A), injection (Fw<0) and shrinking ($\sigma < 0$) parameters.
- The fluid velocity rises as buoyancy parameters (Gr, Gc) increase in values while reverse is the case for temperature and species concentration. More so, the magnetic field and permeability parameters intensify in values as to raise the magnitudes of fluid temperature and species concentration.
- Schmidt number (Sc) as well as the destructive chemical reaction (K>0) increment leads to a fall in not only the local skin friction but also the local Nusselt number. In addition, Sc and Pr reduce the fluid velocity $f(\eta)$ as they separately rise in values.
- Rise in the generative chemical reaction parameter (K<0) causes increment in both fluid velocity and species concentration but increase in heat generation parameter (S>0) raises the fluid velocity and temperature.
- Increase in the stretching parameter decreases both the dimensionless temperature and species concentration but opposite effect are cast by rising shrinking parameter (S<0).
- The local skin friction and reduced local Sherwood number fall in magnitudes when Prandtl number and heat absorption parameter rise in values but the reduced local Nusselt number responds oppositely.
- The reduced local Sherwood number falls in magnitude as the velocity ratio ($\mathcal{E}$) intensifies.

REFERENCES

[1] Adeniyan, A., Ogwuegbu, C. S (2014), Effects of Chemical Reaction and Heat Generation on a Mixed Convection Stagnation Point Flow, Heat and Mass Transfer towards a Stretching Vertical Porous Flat Plate, Asian Research Publishing Network [ARPN] J. Engng. & Appl. Sci., vol. 9, no. 12, pp. 2676-2686

[2] Anderson, J. D (2005), Ludwig Prandtl's boundary layer, American Institute of Physics, Physics Today-S-0031-9228-0512-020-1.

[3] Aziz, A. (2009), A similarity solution for laminar thermal boundary layer over a flat plate with a convective surface boundary condition, Commun. Nonlinear Sci. Numer. Simulat., 14, pp. 1064-1068.

[4] Chamkha, A (1998), Unsteady hydromagnetic flow and heat transfer from a non-isothermal stretching sheet immersed in a porous medium, Int. Comm. Heat Mass Transfer, vol. 25, No. 6, pp. 899-906.

[5] Crane, L. J (1970), Flow past a stretching plate, Z. Angews. Math. Phys. (ZAMP), 21, 645-647.

[6] Damseh, R. A., Duwairi, H. M., Al-Odat, M (2006), Similarity analysis of magnetic field and thermal radiation effects on forced convection flow, Turkish J. Eng. Env. Sci. , 30, pp. 83-89.

[7] Das, K (2011), Effects of heat and mass transfer on MHD free convection flow near a moving vertical plate of a radiating and chemically reacting fluid, Journ. Sib. Feb. Univ. Math. & Phys. 4(1), pp.18-31.

[8] Davidson, P.A (2001), An Introduction to Magnetohydrodynamics, Cambridge Univ. Press, UK

[9] Heck, A (2003), Introduction to Maple, 3rd Edn., Springer-Verlag, New York, Inc.

[10] Hiemenz , K (1911) The Boundary Layer Analysis of a Uniformly Flowing Liquid Circulating in Straight Circular Cylinder (in German), Dinglers Polytech*. J., 326* (1911), pp. 321-324.

[11] Hossain, M. S., Samand, M. A (2013), Heat and mass transfer of an MHD free convection flow along a stretching sheet with chemical reaction, radiation and heat generation in presence of magnetic field, Research Journ. of Mathematics and Statistics, 5(1-2): 05-17.

[12] Ibrahim, S. M (2014), Effects of chemical reaction on dissipative radiative MHD flow through a porous medium over a nonisothermal strtching sheet, Joorn. of Industriam Mathematics, vol. 2014, ID 243148, 10 pages.

[13] Ibrahim, S. M and Reddy, N (2013), Similarity solution of heat and mass transfer for natural convection over a moving vertical plate with internal heat generation and a convective boundary condition in the presence of thermal radiation, viscous dissipation, and chemical reaction, Thermodynamics, Article ID 790604, 10 pages. doi.org/10.1155/790604

[14] Ibrahim, S. Y and Makinde, O. D (2010), Chemically reacting MHD boundary layer flow of heat and mass transfer over a moving vertical plate with suction, Scientific Research and Essays, vol. 5(19), pp. 2875-2882.

[15] Ibrahim, S. Y and Makinde, O. D (2011), Chemically reacting Magnetohydrodynamics (MHD) boundary layer flow of heat and mass transfer past a low-heat-resistant sheet moving vertically downwards, Scientific Research and Essays, vol. 6(22), pp. 4762-4775.

[16] Ishak A, Nazar R, Arifin N.M and Pop I (2007) Mixed convection of a stagnation point flow towards a stretching permeable sheet. Malaysian Journal of Mathematical sciences 1(2) 217-226

[17] Jat, R. N and Chaudhary, S (2009), MHD flow and heat transfer over a stretching sheet, Applied Mathematica Sciences, vol. 3, No. 26, pp. 1285-1294.

[18] Makinde, O. D (2011), Second law analysis for variable viscosity hydromagnetic boundary layer flow with thermal radiation and Newtonian heating, Entropy 13, pp. 1446-1464

[19] Makinde, O. D., Charles, W. M (2010), Computational dynamics of hydromagnetic stagnation flow towards a stretching sheet, Appl. Comput. Math., 9(2), 2010, pp 243 – 251

[20] Makinde, O. D., Olanrewaju, O. D (2012), Combined effects of internal heat generation and buoyancy force on boundary layer flow over a vertical plate with a convective surface boundary condition, Canadian J. of Chem. Engng., vol. 90, pp. 1289-1294.

[21] Makinde, O. D., Zima, K,. Anwar Beg, O (2012), Numerical study of chemically reacting hydromagnetic boundary layer flow with Soret/Dufour effects and a convective surface boundary condition, Int. J. of Thermal & Environmental Engineering, vol. 4, No. 1, pp. 89-98.

[22] Merkin, J. H (1985), On dual solution occurring in mixed convection in a porous medium, Journ. of Engng. Math. , pp. 171-179.

[23] Mukhopadhyay, S (2012): Analysis of boundary layer flow and heat transfer along a stretching cylinder in a porous medium, Int. Sholarly Research Network-Thermodynamics, Article ID 704984, Article ID 704984, 7 pages.
[24] Mukhopadhyay, S (2013): Chemically reactive solute transfer in MHD boundary layer flow along a stretching cylinder with partial slip, Int. J. of Appl. Math. and Mech. 9(1): 62-79
[25] Olanrewaju, P. O., Alao, F. I., Adeniyan, A., Bishop, S. A (2013), Double-diffusive convection from a permeable vertical surface under convective boundary condition in the presence of heat generation and thermal radiation, Nonlinear Sci. Lett. A, vol. 4, No. 3, pp. 76-90
[26] Olanrewaju, P. O., Makinde, O. D (2011), Effects of thermal diffusion and diffusion thermo on chemically reacting MHD boundary layer flow of heat and mass transfer past a moving vertical plate with suction/injection, Ara. J. Sci. Eng, 36, 1607-1619.
[27] Ridha, A (1996), Aiding flows non-unique similarity solutions of mixed convection boundary-layer equations, Z. Angew Math. Phys. (ZAMP), vol. 47, No. 3, pp. 341-352.
[28] Sakiadis, B. C (1961), Boundary layer behavior on continuousln solid surfaces: I. Boundary-layer equations for two-dimensional and axisymmetric flow, AIChE J., 7, 26-28.
[29] Shivamoggi, B. K (1985), Theoretical Fluid Dynamics, Kluwer Academic Publishers, Hingham,
[30] shrinking sheet, Sains Malasiana, vol. 40, no. 10, pp. 1179-1186.
[31] Siegel, R. S., Howell, J. R (1972), Thermal radiation heat transfer, International Student Edn., McGraw-Hill, New York.
[32] Sparrow, E. W., Cess, D. R (1978), Radiation Heat Transfer, Augmented Edition, Hemesphere Publishing Corporation, Washington D.C.
[33] Syed, K. S., Ahmad, S., Ashraf, M (2012), Study of magnetohydrodynamic and thermal characteristics of axisymmetric stagnation point flow with viscous dissipation over a strtching surface, World Applied Sciences J. 18(1): 43-54.USA.
[34] Yian, L. Y., Ishak, A., Pop, A (2011), MHD stagnation point flow with suction towards a

DEPARTMENT OF MATHEMATICS, UNIVERSITY OF LAGOS, LAGOS